Novel Input Current Ripple Compensation Technique for Capacitor-less Dual-Half-Bridge Converter

Changkyu Bai, Byeongcheol Han
POSTECH
Pohang, Gyeongbuk,
South Korea

Dong-Young Huh, Jung-Hwan Choi, and Soo-Hong Kim
LG Innotek
Ansan, Gyeonggi,
South Korea

Jin S. Lee, and Minsung Kim*
POSTECH
Pohang, Gyeongbuk,
South Korea
Email: redtoss@postech.ac.kr

***Abstract*— This paper proposes a repetitive controller to be used for capacitor-less current-fed dual-half-bridge (CF-DHB) converters under the grid-connected environment. When the dc-link capacitor is very small, the dc-link current fluctuation can distort the input current severely. Compared with the previous controllers introduced to reduce the input current ripples, the proposed repetitive controller can reduce them more significantly. In developing the proposed controller, we derived the dynamic model of the capacitor-less CF-DHB in the grid-connected environment, and used it to implement the repetitive controller. Experimental results verify that the proposed control scheme achieves desirable performance.**

***Index Terms*—Two-stage inverter, input current ripple, dc-dc converter, controller design**

I. Introduction

Fuel cell technology is a prospective candidate that can replace the current internal combustion engines in the traditional cars and the conventional batteries used in the today's electric vehicles, and becomes one of the primary micro-grid power sources. It offers high efficiency, low emissions of regulated pollutants, and excellent part-load performance [1]. Most of the present fuel cell stack modules produce the output voltage range from 24 V to 150 V. To enable the fuel-cell stack to be used in the grid-connected environment, we need to adopt the high step-up converter that is able to boost the low dc voltage to the high dc voltage.

Among the step-up converters used for fuel cell power conditioning system, the current-fed dual-half-bridge (CF-DHB) converter is considered the attractive alternative due to its low-input current ripple, low-cost and high conversion efficiency [3]. When the dc load is connected to a CF-DHB converter, the dc load current does not have a low-frequency current ripple that may affect the hysteresis behavior in the fuel cell environment and the thermal problem among stacks. But, as the ac grid is connected to the fuel-cell stack, the fuel cell current will have a double-frequency ripple current generated by the inverter load. The current ripple with the frequency under 400 Hz is able to impair the fuel cell stack. To reduce the current ripple on the fuel cell, a bulky electrolytic capacitor is usually used as the energy buffer to reduce the current ripple with 120 Hz [2]. However, the electrolytic capacitor would increase the system volume and cost as well as decrease the system lifetime.

To reduce the low-frequency current ripple on the fuel cell without having to use the large electrolytic capacitors, a high-gain proportional-integral (PI) controller can be used. As the high-gain PI controller increases the gain around 120 Hz, we can easily reduce the current ripple. However, this controller also increases the system magnitude in the high-frequency region and decreases the phase margin. Since then, PR controller has been developed [4, 5]. It acts as a notch filter to eliminate the grid voltage disturbance at the fundamental and harmonic frequencies. However, the PR controller provides infinite gain at only a selected resonant frequency, so the parallel use of the multiple PR controllers is required to compensate several frequency components such as the grid and its harmonics frequencies; this fact increases complexity in the digital implementation and causes heavy computation burden. Moreover, the PR controller constructs the control input by using the current error only and thus, the control accuracy is not much improved.

To overcome the aforementioned problem, we propose to use a repetitive controller for capacitor-less CF-DHB converters. The repetitive control algorithm has been widely used as a solution to track a periodic signal and to eliminate periodic disturbances in dynamic systems [6]-[12]. It uses information obtained from the previous trial to repetitively adjust the current control inputs, and consequently generates a series of control inputs such that the tracking errors converge to zero. The repetitive controller is computationally simple and easy to implement. In developing the proposed controller, we derived the dynamic model of the capacitor-less CF-DHB in the grid-connected environment, and used it to implement the repetitive controller. We also provide detailed and practical design guidelines of the control parameters to develop a CF-DHB converter. The proposed repetitive controller is able to reduce the input current ripple significantly. Experimental results verify that the proposed control scheme achieves desirable performance.

978-1-5090-5366-7/17/$31.00

This paper is organized as follows. The CF-DHB converter with the H-bridge inverter are described in Section II, and a control scheme suited to the CF-DHB converter is proposed in Section III. The experimental setup and results are presented in Section IV. Finally, conclusions are drawn in Section V.

II. Preliminary and Problem Formulation

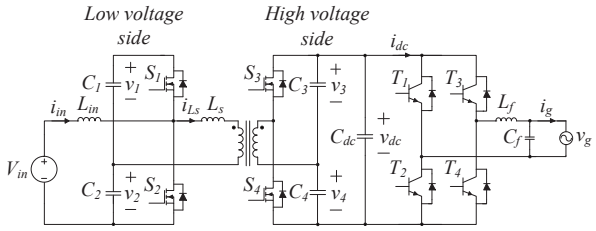

Fig. 1. Grid-connected power conversion system for fuel-cell, in which CF-DHB topology is used in the dc-dc stage.

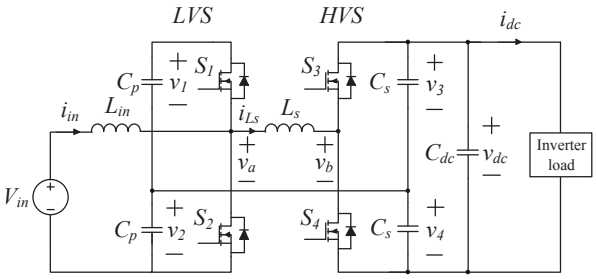

Fig. 2. Equivalent circuit of CF-DHB converter.

The proposed grid-connected system for fuel-cell is composed of two parts: CF-DHB converter and H-bridge inverter (Fig. 1). The CF-DHB converter boosts the low input voltage to the high output voltage, and the H-bridge inverter transforms the DC output of the CF-DHB converter into the AC power with the line frequency. The CF-DHB converter part consists of input inductor L_{in}, low voltage side (LVS) switches S_1, S_2, capacitors C_1, C_2, ideal transformer T with turns ratio $n = N_p/N_s$, transformer leakage inductor L_s, high voltage side (HVS) switch S_3, S_4, capacitor C_3, C_4, and dc link capacitor C_{dc}. V_{in} and v_{dc} represent respectively the input and output voltage. i_{in} and i_{dc} represent respectively the input and output current. As the power flows from LVS to the HVS, the circuit operates in boost mode to keep the HVS voltage at a desired high value. In the other direction of power flow, the circuit operates in buck mode to absorb regenerated energy. The H-bridge inverter consists of four switches T_1, T_2, T_3, T_4, filter inductor L_f, and filter capacitor C_f. v_g and i_g represent the rectified grid voltage and current respectively.

Assume that the transformer turns ratio is one (i.e. $N_p = N_s$). Primary capacitors and secondary capacitors are set as follow $C_p = C_1 = C_2$, $C_s = C_3 = C_4$. Then, simply regarding the transformer as leakage inductance L_s, we obtain the equivalent circuit of the CF-DHB converter as shown in Fig. 2. The circuit uses the transformer leakage inductance L_s as energy transfer element and an interface between LVS and HVS half-bridges. The circuit is designed to operate by the phase shift angle Φ between the switches of LVS and HVS half bridges.

A. Dynamic modeling of CF-DHB converter

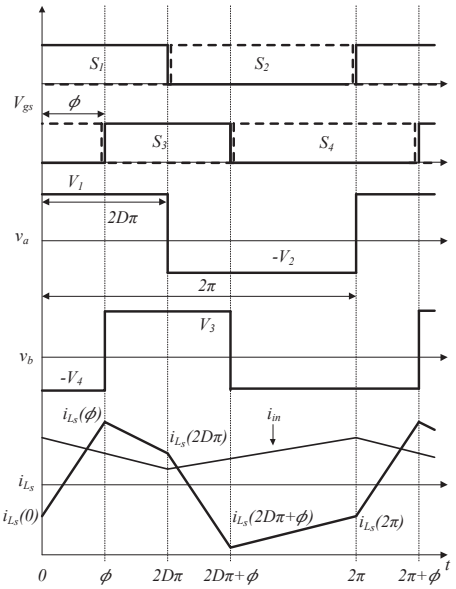

Fig. 3. Theoretical waveforms of the CF-DHB converter.

The CF-DHB converter experiences four phases per switching period: 1) S_2 turned off and S_1 turned on; 2) S_4 turned off and S_3 turned on; 3) S_1 turned off and S_2 turned on; 4) S_3 turned off and S_4 turned on (Fig. 1,2). Based on Fig. 3, we can obtain four operation modes in a duty cycle where $D = 0.5$.

$$
\begin{aligned}
i_{L_s}(\theta) &= i_{L_s}(0) + \frac{v_1 + v_4}{\omega L_s}\theta, \quad \text{where } 0 < \theta < \phi, \\
i_{L_s}(\theta) &= i_{L_s}(\phi) + \frac{v_1 - v_3}{\omega L_s}(\theta - \phi), \quad \text{where } \phi < \theta < \pi, \\
i_{L_s}(\theta) &= i_{L_s}(\pi) + \frac{-v_2 - v_3}{\omega L_s}(\theta - \pi), \\
&\qquad \text{where } \pi < \theta < \pi + \phi, \\
i_{L_s}(\theta) &= i_{L_s}(\pi + \phi) + \frac{-v_2 + v_4}{\omega L_s}(\theta - \pi - \phi), \\
&\qquad \text{where } \pi + \phi < \theta < 2\pi. \qquad (1)
\end{aligned}
$$

By solving (1), the initial conditions of $i_{L_s}(t)$ at $t = 0, \phi, \pi, \pi + \phi$ can be obtained as

$$
\begin{aligned}
i_{L_s}(0) &= \frac{v_3 - v_1}{2\omega L_s}(\pi - \phi) - \frac{v_1 + v_4}{2\omega L_s}\phi, \\
i_{L_s}(\phi) &= \frac{v_1 + v_4}{2\omega L_s}\phi + \frac{v_3 - v_1}{2\omega L_s}(\pi - \phi), \\
i_{L_s}(\pi) &= -i_{L_s}(0), \\
i_{L_s}(\pi + \phi) &= -i_{L_s}(\phi). \qquad (2)
\end{aligned}
$$

The state-space equations of CF-DHB converter for the four phases is derived as follows:

Phase 1 ($0 < \theta < \phi$):

$$\dot{\mathbf{x}}(t) = \begin{bmatrix} 0 & -1/L_{in} & 0 \\ 2/C_p & 0 & 0 \\ 0 & 0 & 0 \end{bmatrix} \mathbf{x}(t) + \begin{bmatrix} V_{in}/L_{in} \\ -i_{L_s}/C_p \\ -i_{L_s}/(C_s+2C_{dc}) - 2i_{dc}/(C_s+2C_{dc}) \end{bmatrix}. \quad (3)$$

Phase 2 ($\phi < \theta < \pi$):

$$\dot{\mathbf{x}}(t) = \begin{bmatrix} 0 & -1/L_{in} & 0 \\ 2/C_p & 0 & 0 \\ 0 & 0 & 0 \end{bmatrix} \mathbf{x}(t) + \begin{bmatrix} V_{in}/L_{in} \\ -i_{L_s}/C_p \\ i_{L_s}/(C_s+2C_{dc}) - 2i_{dc}/(C_s+2C_{dc}) \end{bmatrix}. \quad (4)$$

Phase 3 ($\pi < \theta < \pi + \phi$):

$$\dot{\mathbf{x}}(t) = \begin{bmatrix} V_{in}/L_{in} \\ i_{L_s}/C_p \\ i_{L_s}/(C_s+2C_{dc}) - 2i_{dc}/(C_s+2C_{dc}) \end{bmatrix}. \quad (5)$$

Phase 4 ($\pi + \phi < \theta < 2\pi$):

$$\dot{\mathbf{x}}(t) = \begin{bmatrix} V_{in}/L_{in} \\ i_{L_s}/C_p \\ -i_{L_s}/(C_s+2C_{dc}) - 2i_{dc}/(C_s+2C_{dc}) \end{bmatrix}. \quad (6)$$

where $\mathbf{x}(t) = [i_{in}(t), v_{12}(t), v_{34}(t)]^T$ is the state vector, and $v_{12}(t)$ and $v_{34}(t)$ are $v_1(t) + v_2(t)$ and $v_3(t) + v_4(t)$ respectively.

Using the state-space averaging method and the integration of fast variable $i_{L_s}(t)$ for each phase based on (1)-(2), we can derive the average model

$$\dot{\mathbf{x}}(t) = \begin{bmatrix} 0 & -\frac{1}{2L_{in}} & 0 \\ \frac{1}{C_p} & 0 & \frac{-2\phi(\pi-\phi)}{C_p T_s 2\omega^2 L_s} \\ 0 & \frac{2\phi(\pi-\phi)}{C_t T_s 2\omega^2 L_s} & 0 \end{bmatrix} \mathbf{x} + \begin{bmatrix} \frac{V_{in}}{L_{in}} \\ 0 \\ \frac{-2i_{dc}}{C_t} \end{bmatrix},$$
$$\mathbf{y}(t) = \begin{bmatrix} 1 & 0 & 0 \\ 0 & 0 & 1 \end{bmatrix} \mathbf{x}(t), \quad (7)$$

where $\phi(t)$, $i_{dc}(t)$ are the control input phase and dc-link current, $\mathbf{y}(t) = [i_{in}(t), v_{34}(t)]^T$ are the output vector, and $C_t = C_s + 2C_{dc}$.

Linearizing the average model (7) yields the small-signal model

$$\dot{\hat{\mathbf{x}}}(t) = \begin{bmatrix} 0 & -\frac{1}{2L_{in}} & 0 \\ \frac{1}{C_p} & 0 & \frac{-2\Phi(\pi-\Phi)}{C_p T_s 2\omega^2 L_s} \\ 0 & \frac{2\Phi(\pi-\Phi)}{C_t T_s 2\omega^2 L_s} & 0 \end{bmatrix} \hat{\mathbf{x}}(t) + \begin{bmatrix} 0 & 0 \\ \frac{(-2\pi+4\Phi)V_{34}}{C_p T_s 2\omega^2 L_s} & 0 \\ \frac{(2\pi-4\Phi)V_{12}}{C_t T_s 2\omega^2 L_s} & -\frac{2}{C_t} \end{bmatrix} \cdot \begin{bmatrix} \hat{\phi}(t), \\ \hat{i}_{dc}(t) \end{bmatrix},$$
$$\hat{\mathbf{y}}(t) = \begin{bmatrix} 1 & 0 & 0 \\ 0 & 0 & 1 \end{bmatrix} \dot{\hat{\mathbf{x}}}(t), \quad (8)$$

where $\hat{\mathbf{x}}(t) = [\hat{i}_{in}(t), \hat{v}_{12}(t), \hat{v}_{34}(t)]^T$ and $\hat{\mathbf{y}}(t)$ are the incremental variations of $\mathbf{x}(t)$ and $\mathbf{y}(t)$ respectively. $\hat{i}_{in}(t)$, $\hat{v}_{12}(t)$, $\hat{v}_{34}(t)$ and $\hat{\phi}(t)$ are respectively the incremental variations of $i_{in}(t)$, $v_{12}(t)$, $v_{34}(t)$, $\phi(t)$, $i_{dc}(t)$. And, I_{in} V_{12}, V_{34}, Φ, I_{dc} are the operating points of $i_{in}(t)$, $v_{12}(t)$, $v_{34}(t)$, $\phi(t)$, and $i_{dc}(t)$.

Based on the above small-signal models (8), we can obtain the transfer functions from $\hat{\phi}(s)$ to $\hat{i}_{in}(s)$ and $\hat{v}_{34}(s)$ and from $\hat{i}_{dc}(s)$ to $\hat{i}_{in}(s)$ as

$$G_{i\phi}(s) = \frac{\hat{i}_{in}(s)}{\hat{\phi}(s)} = \frac{a_1 s + a_2}{b_1 s^3 + b_2 s}, \quad (9)$$

$$G_{v\phi}(s) = \frac{\hat{v}_{34}(s)}{\hat{\phi}(s)} = \frac{c_1 s^2 + c_2 s + c_3}{e_1 s^3 + e_2 s}, \quad (10)$$

$$G_{io}(s) = \frac{\hat{i}_{in}(s)}{\hat{i}_{dc}(s)} = \frac{f_1}{g_1 s^3 + g_2 s}, \quad (11)$$

where the derived parameters a_i and g_i for $i = 1, 2$, b_j and e_j for $j = 1, ..., 4$, c_k for $k = 1, ..., 3$, and f_1 are given in Appendix A.

To develop the controller in the discrete-time domain, we need to derive the small-signal models in the discrete-time domain. Using the backward difference method with the switching period T_s, we can represent the discrete-time transfer functions as

$$G_{i\phi}(z) = \frac{\hat{i}_{in}(z)}{\hat{\phi}(z)} = \frac{h_1 z^3 + h_2 z^2}{k_1 z^3 + k_2 z^2 + k_3 z + k_4}, \quad (12)$$

$$G_{v\phi}(z) = \frac{\hat{v}_{34}(z)}{\hat{\phi}(z)} = \frac{l_1 z^3 + l_2 z^2 + l_3 z}{m_1 z^3 + m_2 z^2 + m_3 z + m_4}, \quad (13)$$

$$G_{io}(z) = \frac{\hat{i}_{in}(z)}{\hat{i}_{dc}(z)} = \frac{p_1 z^3}{q_1 z^3 + q_2 z^2 + q_3 z + q_4}, \quad (14)$$

where the derived parameters h_i for $i = 1, 2$, k_j, m_j, and q_j for $j = 1, ..., 4$, l_k for $k = 1, ..., 3$, and p_1 are also given in Appendix A.

III. Control scheme

A. Conventional controller

The control objective of the CF-DHB converter is to make the input current track the desired value as closely as possible. To stabilize the CF-DHB converter, we first can use a conventional proportional-integral (PI) controller.

The transfer function of the PI controller is represented as

$$C_{fb}(z) = k_p + k_i \frac{T_s}{1 - z^{-1}}, \quad (15)$$

where k_p is the proportional controller gain, k_i is the integral controller gain.

Fig. 4 shows the Bode plot of the PI control system using the parameters listed in Table I and the PI control gains determined in the following simulation section. As shown in Fig. 4, the high-gain PI controller increases the gain around 120 Hz, thereby improving the accuracy of tracking and disturbance rejection. However, the controller also increases the system gain in the high-frequency region and decreases the phase margin. To

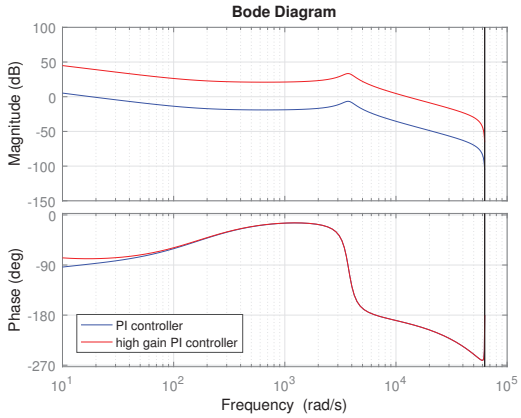

Fig. 4. Bode plots of $G_{i\phi}(z)$ when only PI controllers are used: PI controller where control gains are tuned by 'PID tuner' (blue), and high-gain PI controller (red).

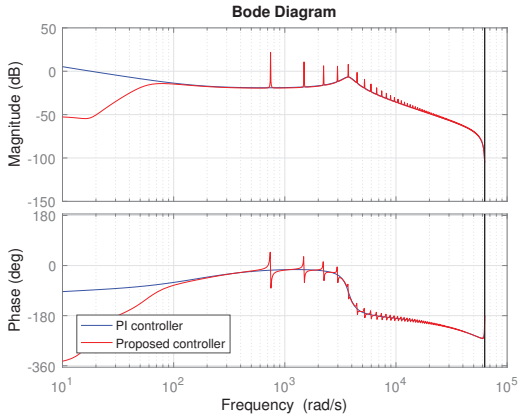

Fig. 5. Bode plots of $G_{i\phi}$ when only PI controller is used: PI controller where control gains are tuned by 'PID tuner' (blue) and when the proposed repetitive controller is used (red).

overcome the problem, we propose to use the repetitive controller.

B. Repetitive controller design

The repetitive controller is usually used in a system that performs the same task repetitively. The knowledge obtained from the previous trial is used to improve the control signal for the current trial. The control signal in each trial is adjusted using the tracking error signals obtained from previous trial and theoretically achieves zero tracking error. The proposed repetitive controller for the CF-DHB is described as

$$C_{rc}(z) = k_r \frac{z^{-N}Q(z)}{1 - z^{-N}Q(z)}, \tag{16}$$

where k_r is the RC gain; $N = f_s/f_r$ where $f_s = 1/T_s$ and f_r are respectively the switching and ripple frequencies; $Q(z)$ is the low-pass filter to suppress the high frequency noise; For implementation simplicity, we choose to use the first-order low-pass filter as a candidate

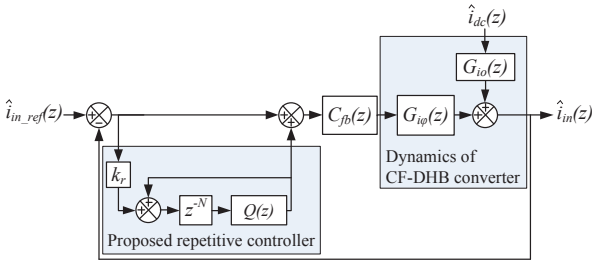

Fig. 6. The schematic diagram the CF-DHB converter control system. $\hat{i}_{in\_ref}(z)$ is reference input current.

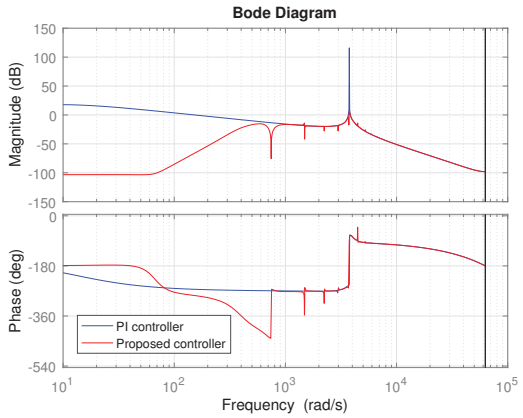

Fig. 7. Bode plots of G_{io} when only PI controller is used: PI controller where control gains are tuned by 'PID tuner' (blue) and when the proposed repetitive controller is used (red).

for $Q(z)$:

$$Q(z) = \frac{1}{\tau \frac{(1-z^{-1})}{T_s} + 1}, \tag{17}$$

where $\tau = 1/2\pi f_{lp}$ with cut-off frequency f_{lp} (Hz).

The proposed dynamic control system is shown in Fig. 6. This control scheme consists of two components: the PI control term that forces the closed-loop system stay within a uniform bound; the repetitive controller term that suppresses the residual disturbances and enhances the command input response.

In the above closed-loop system, the load disturbance to the input current transfer function can be obtained as follows:

$$G_{io\_cl}(z) = \frac{\hat{i}_{in}(z)}{\hat{i}_{dc}(z)} = \frac{G_{io}(z)}{1 + C_{rc}(z)C_{fb}(z)G_{i\phi}(z)}. \tag{18}$$

This transfer function describes the effect of dc-link current fluctutation to the input current.

Fig. 6 shows the Bode plot of the repetitive control system using the parameters listed in Table I and the repetitive control gains determined in the following simulation section. As shown in Fig. 5, the repetitive controller increases the system gain around $\omega_l = 2\pi l f_r$, with $l = 0, 1, 2, ..., L$ without reducing the phase margin. Thus, it can suppress the 120Hz input current disturbance

from the inverter load. Fig. 7 shows the disturbance rejection ability more clearly. The system gain around $\omega_l = 2\pi l f_r$ become significantly decreased, which means that the disturbance around $\omega_l = 2\pi l f_r$ can be effectively suppressed. Consequently, almost constant input current can be attained without having to use large dc-link capacitor.

IV. Experiment

TABLE I
PARAMETERS AND COMPONENTS OF THE CF-DHB CONVERTER

Parameters	Symbols	Values
Input voltage	V_{in}	50 V_{dc}
DC link voltage	v_{dc_ref}	380 V_{dc}
Grid voltage	v_g	220 V_{rms}
Grid frequency	f_g	60 Hz
Ripple frequency	f_r	120 Hz
Transformer turns ratio	$N_p : N_s$	16:64
Switching frequency	f_s	20 kHz
Primary capacitance	C_p	300 μF
Secondary capacitance	C_s	100 μF
DC-link capacitance	C_{dc}	100μF(*3.3mF)
Input inductance	L_{in}	118.4 μH
Leakage inductance	L_s	12.8 μF
Filter capacitance	C_f	1.41 μF
Filter inductance	L_f	4 mF
Components	**Symbols**	**Part numbers**
Primary Switch	S_1, S_2	IPA045N10N3G
Secondary Switch	S_3, S_4	IPW65R190CFD
Transformer core	T	PQ4040
H-Bridge Switch	$T_1 - T_4$	FGY75N60SMD

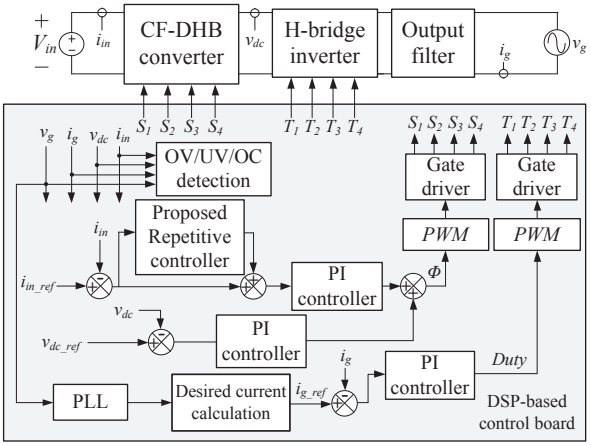

Fig. 8. Configuration of the proposed control system. PWM, PLL, OV, UV, and OC stand for pulse-width modulation, phase locked loop, over voltage, under voltage, and over current, respectively.

A 500-W experimental CF-DHB converter (Fig. 8, Table I) was constructed to demonstrate the feasibility of the proposed controller. In the experimental setup, the nominal input voltage and the rated power were set to 50 V and 500 W. The control algorithms were implemented on a TMX320F28377D digital controller, which is protected by using the phase-locked loop (PLL) and the current overflow protection algorithm.

Using the CF-DHB converter model (Eqs. (12), (13), (14)), we designed the proposed RC for the developed CF-DHB converter. At the instantaneous peak power of 500 W with full load, the transfer function of the CF-DHB converter becomes

$$G_{i\phi}(z) = \frac{1.824z^2 - 0.005103z - 1.788}{z^3 - 2.924z^2 + 2.883z - 0.9586}, \quad (19)$$

$$G_{v\phi}(z) = \frac{17.45z^2 - 33.72z + 16.87}{z^3 - 2.924z^2 + 2.833z - 0.9586}, \quad (20)$$

$$G_{io}(z) = \frac{-(4.951z^2 + 19.77z + 4.951)10^{-5}}{z^3 - 2.965z^2 + 2.965z - 1}. \quad (21)$$

The PI controllers are then designed to satisfy the design criterion: phase margin 90°, maximum overshoot 0.05, response time 0.12 s. The controller gains are tuned using the "PID Tuner" available in MATLAB. The desired phase margin is set to 90° to guarantee system robustness. As a result, PI controller gains are obtained as $k_p = 0.001$ and $k_i = 0.003$. The parameter design procedure of the repetitive controller is described as follows. To suppress the fundamental and low-order harmonic components at over 2 kHz frequency, we select the cutoff frequency of $Q(z)$ at f_c = 2 kHz. To make the G_{io} system gain less than -60 dB at multiples of 120 Hz frequencies, the repetitive controller gain is set to k_r = 0.001.

To evaluate the control accuracy of the repetitive controller, we first conducted the experiment with $C_{dc} = 3.3$ mF and the equivalent dc bus capacitor $C_{eq} = 3.35$ mF. Fig. 9(a) shows the waveforms of dc-link voltage, grid current, grid voltage, input current when the PI controller is used. The dc-link voltage and input current does not show any noticeable fluctuations. We decrease the value of dc-link capacitor to 100 μF and the equivalent dc bus capacitor $C_{eq} = 0.15$ mF. Fig. 9(b) shows the waveforms of dc-link voltage, grid current, grid voltage, input current when the PI controller is used. The dc-link voltage and input current highly fluctuates with 120 Hz frequency ripple as shown in Fig. 9(b). We now applied the proposed repetitive controller to the CF-DHB converter with $C_{dc} = 100\ \mu F$. Fig. 9(c) shows the waveforms of dc-link voltage, grid current, grid voltage, input current when proposed repetitive controller is used. Even though the magnitude of dc-link voltage ripple increases from 18 V to 20 V, the input current ripple dramatically decreases from 9 A to less than 1 A.

V. Conclusion

This paper proposed a CF-DHB converter control system that can achieve low-frequency ripple-free input current using a RC controller under the grid connected environment. The implementation of the proposed control scheme is mainly achieved by controlling the phase shift of the CF-DHB converter. The RC controller is developed to achieve high control gain at 120 Hz frequency to eliminate double-frequency ripple input current. The controller design guideline was suggested based on the developed converter small-signal model. The performance

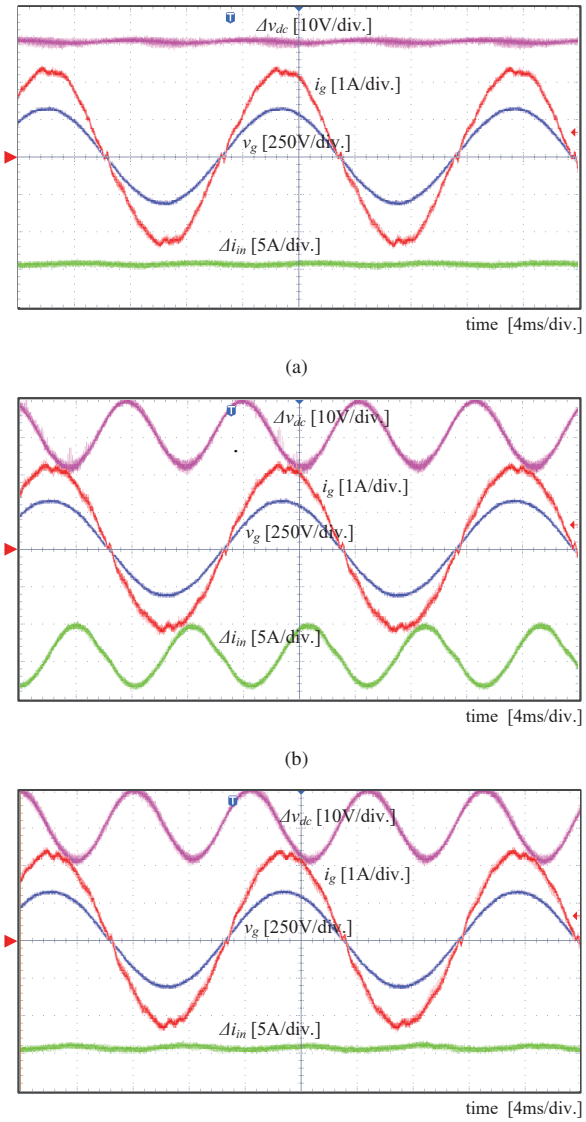

Fig. 9. Experimental waveforms of dc-link voltage, grid current, grid voltage, input current. (a) When the PI controller is used with $C_{dc} = 3.3$ mF, (b) When the PI controller is used with $C_{dc} = 100$ μF, (c) When the RC is used with $C_{dc} = 100$ μF.

of the proposed technology is verified experimentally by using the 500-W fuel cell system.

ACKNOWLEDGE

This research was supported by the MSIP (Ministry of Science, ICT and Future Planning), Korea, under the "ICT Consilience Creative Program" (IITP-R0346-16-1007) supervised by the IITP (Institute for Information & communications Technology Promotion) and in part by a grant (#S0417-16-1004) from Regional Software Convergence Products Commercialization Project funded by MSIP and NIPA (National IT Industry Promotion Agency).

REFERENCES

[1] X. Yu, M. Starke, L. Tolbert, and B. Ozpineci, "Fuel cell power conditioning for electrical power application: A summary," *IET Electr. Power Appl.*, vol. 1, no. 5, pp. 643-656, Sep. 2007.

[2] X. Yu, M. Starke, L. Tolbert, and B. Ozpineci, "Fuel cell power conditioning for electrical power applications: A summary," *IET Electr. Power Appl.*, vol. 1, no. 5, pp. 643–656, Sep. 2007.

[3] H. Li and F. Z. Peng, "Modeling of a New ZVS Bi-directional DC-DC Converter," *IEEE Trans. Aero. and Electronc. Sys.*, vol. 40, no. 1, pp. 272–283, Jan. 2004.

[4] D. B. W. Abeywardana, B. Hredzak, and V. G. Agelidis, "An input current feedback method to mitigate the dc-side low-frequency ripple current in a single-phase boost inverter," *IEEE Trans. Power Electron.*, vol. 31, no. 6, pp. 4594-4603, Jun. 2016.

[5] L. Cau, K. H. Loo, and Y. M. Lai, "Frequency-adaptive filtering of low-frequency harmonic current in fuel cell power conditioning systems," *IEEE Trans. Power Electron.*, vol. 30, no. 4, pp. 1966-1978, Apr. 2015.

[6] Y. Cho and J. Lai, "Digital plug-in repetitive controller for single-phase bridgeless PFC converters," *IEEE Trans. Power Electron.*, vol. 28, no. 1, pp. 165-175, Jan. 2013.

[7] B. Zhang, K. Zhou and D. Wang, "Multirate Repetitive Control for PWM DC/AC Converters," *IEEE Trans. Ind. Electron.*, vol. 61, no. 6, pp. 2883-2890, Jun. 2014.

[8] H. Deng, R. Oruganti and D. Srinivasan, "Analysis and Design of Iterative Learning Control Strategies for UPS Inverters," *IEEE Trans. Ind. Electron.*, vol. 54, no. 3, pp. 1739-1751, Jun. 2007.

[9] J. Liu, P. Zanchetta, M. Degano and E. Lavopa, "Control design and implementation for high performance shunt active filters in aircraft power grids," *IEEE Trans. Ind. Electron.*, vol. 59, no. 9, pp. 3604-3613, Sep. 2012.

[10] P. Zanchetta, M. Degano, J. Liu and P. Mattavelli, "Iterative Learning Control With Variable Sampling Frequency for Current Control of Grid-Connected Converters in Aircraft Power Systems," *IEEE Trans. Ind. Electron.*, vol. 49, no. 4, pp. 1548-1555, Jul./Aug. 2013.

[11] Kim, S., Lee, S. H., Lee, J. S., and Kim, M., "Dual-Mode Flyback Inverters in Grid-Connected Photovoltaic Systems," *IET Renew. Power Gen., (Accepted for publication: DOI: 10.1049/iet-rpg.2015.0491)*

[12] Kim, H., Lee, J. S., Lai, J. S., and Kim, M., "Iterative Learning Controller with Multiple Phase-Lead Compensation for Dual-Mode Flyback Inverter," *IEEE Trans. Power Electron., (Accepted for publication: DOI: 10.1109/TPEL.2016.2614602)*

APPENDIX A

The parameters used in (9)-(14) are given as

$$a_1 = -C_t L_s T_s V_{34} \omega^2 (2\Phi - \pi), \tag{22}$$
$$a_2 = -V_{12}(-\Phi^2 + \pi\Phi)(2\Phi - \pi), \tag{23}$$
$$b_1 = 2C_p C_t L_{in} L_s^2 T_s^2 \omega^4, \tag{24}$$
$$b_2 = C_t L_s^2 T_s^2 \omega^4 + 2L_{in}\Phi^4 - 4L_{in}\Phi^3\pi + 2L_{in}\Phi^2\pi^2, \tag{25}$$
$$c_1 = -2C_p L_{in} L_s T_s V_{12}(2\Phi - \pi)\omega^2, \tag{26}$$
$$c_2 = -V_{34}(2L_{in}\Phi^2 - 2L_{in}\Phi\pi)(2\Phi - \pi), \tag{27}$$
$$c_3 = -L_s T_s V_{12}(2\Phi - \pi)\omega^2, \tag{28}$$
$$e_1 = 2C_p C_t L_{in} L_s^2 T_s^2 \omega^4, \tag{29}$$
$$e_2 = C_t L_s^2 T_s^2 \omega^4 + 2L_{in}\Phi^4 - 4L_{in}\Phi^3\pi + 2L_{in}\Phi^2\pi^2, \tag{30}$$
$$f_1 = -2\Phi(\pi - \Phi) T_s \omega^2 L_s, \tag{31}$$
$$g_1 = 2C_p C_t L_{in} L_s^2 T_s^2 \omega^4, \tag{32}$$
$$g_2 = C_t L_s^2 T_s^2 \omega^4 + 2L_{in}\Phi^4 - 4L_{in}\Phi^3\pi + 2L_{in}\Phi^2\pi^2, \tag{33}$$
$$h_1 = T_s^2(a_1 + T_s a_2), \tag{34}$$
$$h_2 = -T_s^2 a_1, \tag{35}$$
$$k_1 = b_2 T_s^2 + b_1, \tag{36}$$
$$k_2 = -b_2 T_s^2 - 3b_1, \tag{37}$$
$$k_3 = 3b_1, \tag{38}$$
$$k_4 = -b_1, \tag{39}$$
$$l_1 = T_s(c_3 T_s^2 + c_2 T_s + c_1), \tag{40}$$
$$l_2 = -T_s(2c_1 + T_s c_2), \tag{41}$$
$$l_3 = T_s c_1, \tag{42}$$
$$m_1 = e_2 T_s^2 + e_1, \tag{43}$$
$$m_2 = -e_2 T_s^2 - 3e_1, \tag{44}$$
$$m_3 = 3e_1, \tag{45}$$
$$m_4 = -e_1, \tag{46}$$
$$p_1 = f_1 T_s^3, \tag{47}$$
$$q_1 = g_2 T_s^2 + g_1, \tag{48}$$
$$q_2 = -g_2 T_s^2 - 3g_1, \tag{49}$$
$$q_3 = 3g_1, \tag{50}$$
$$q_4 = -g_1. \tag{51}$$